

BEAM ACCELERATION AND TRANSITION CROSSING IN THE FERMILAB BOOSTER*

V. A. Lebedev[†], J.-F. Ostiguy, C.M. Bhat
Fermilab, Batavia, IL, USA

Abstract

To suppress eddy currents, the Fermilab rapid cycling Booster synchrotron has no beam pipe; rather, its combined function dipoles are evacuated, exposing the beam directly to the magnet laminations. This arrangement significantly increases the resistive wall impedance of the dipoles and, in combination with the space charge impedance, substantially complicates longitudinal dynamics at transition. Voltage and accelerating phase profiles in the vicinity of transition are typically empirically optimized to minimize beam loss and emittance growth. In this contribution, we present results of experimental studies of beam acceleration near transition. Using comparisons between observed beam parameters and simulations, we obtain accurate calibrations for the rf program and extract quantitative information about parameters of relevance to the Booster laminated magnets longitudinal impedance model. The results are used to analyse transition crossing in the context of a future 50% increase in beam intensity planned for PIP-II, an upgrade of the Fermilab accelerating complex.

INTRODUCTION

Over the 40 years existence of Fermilab Booster the beam intensity has increased steadily to respond to the demands of the experimental program. In recent years this pace has increased to accommodate a succession of neutrino experiments. To meet the needs of the LBNF/DUNE experimental program, the next planned upgrade of the Fermilab accelerating complex referred to as PIP-II, calls for an additional 50% increase in beam intensity.

Early on, transition crossing has been identified as a machine performance bottleneck. Although transition crossing has evolved into a sophisticated and well-tuned operational procedure, an increase in intensity beyond the current level requires quantitative understanding of all effects driving the process. In this paper we present results of studies aimed at understanding the dynamics of beam acceleration and transition crossing in sufficient details to construct a model with predictive ability. The model aims not only at investigating the impact of an intensity increase on performance, but also at investigating ways to minimize beam loss and emittance growth due to transition crossing.

It is well-known that a jump in accelerating phase from ϕ_{acc} to $\pi - \phi_{acc}$ is required to preserve longitudinal motion stability. In the absence of beam induced forces and motion non-linearity the dynamics below and above transition is symmetric resulting in no emittance growth at transition.

* Work performed for Fermi Research Alliance, LLC under Contract No. DE-AC02-07CH11359 with the United States Department of Energy
[†] val@fnal.gov

In practice the beam induced forces, break this symmetry as well as motion linearity. The result is an intensity dependent focussing mismatch and non-linear distortions of the bunch phase space. The subsequent synchrotron oscillations lead to filamentation and emittance growth.

In contrast to other fast cycling proton synchrotrons, the Fermilab Booster has no dedicated vacuum chamber inside its dipoles; rather, the entire volume between the magnet poles is evacuated. While this arrangement eliminates the issues associated with eddy currents induced by the time-varying bend field in a conventional chamber, having the beam directly exposed to the pole laminations substantially increases the wall impedance. The bunch length achieves its minimum at transition. The corresponding increase in peak current causes an increase in beam induced voltage. The very low synchrotron frequency enhances the non-linearity contribution to emittance growth.

Table 1 presents Booster parameters relevant to beam acceleration and transition crossing.

Table 1: Major Booster Parameters

Injection energy	0.4 GeV
Extraction energy	8 GeV
Ramp rate	15 Hz
Harmonic number	84
Circumference	474.2 m
Momentum compaction	0.03346
Maximum rf voltage	1.2 MeV
RF frequency swing	37.9-52.8 MHz
Number of bunches	82
Nominal beam intensity	$4.2 \cdot 10^{12}$

MEASUREMENTS

To minimize problems with possible signal distortion in electronics and data acquisition as well as possible miscalibrations, raw signals were acquired from a resistive wall monitor (RWM) and from the circuit presenting the analog sum of rf voltages for all cavities (RFSUM). In addition, the signal from a beam position monitor used by the radial position feedback system (RPOS) was recorded. The data were acquired with a multi-channel digital oscilloscope. A sampling rate of 1.2 GHz was selected so as to measure both voltage waveform and the longitudinal density distribution with sufficient resolution. The RWM and RFSUM signals completely characterize the beam behaviour in the longitudinal plane including the amplitude and phase of the accelerating voltage. As will be seen below, the RPOS signal provides accurate calibrations of the rf voltage and phase. Because of the oscilloscope memory limit of $4.5 \cdot 10^6$ samples, the duration of each measurement was set to 3.6 ms. Since this interval is much shorter than the complete 33.3 ms accelerating cycle, data were acquired only during

two time intervals of interest: (1) immediately after injection, when adiabatic bunching occurs and (2) at transition. Beam intensities ranged from $1.2 \cdot 10^{12}$ to $4.8 \cdot 10^{12}$ particles and two sets of data were acquired for each intensity value. Good reproducibility at each intensity was observed in spite of a time jitter ranging from 0 to 18 turns observed in the course of these measurements.

Data analysis was performed into two phases. First, at each turn the arrival time, rms width and peak amplitude of individual bunches were determined from the RWM signal, while the zero-crossing time and amplitude for each period of rf voltage were determined from the RFSUM signal. Accounting for instrumentation offsets, individual bunch profiles were fitted to a truncated Gaussian while each rf period was fitted to a sinusoid. The difference between the bunch arrival time and the zero crossing time for rf (Figure 1) was used to extract the accelerating phase. After verifying that all bunches - including bunches near a two-bunch gap used for extraction - behaved similarly, the data was averaged over all bunches on a turn-by-turn basis. This significantly improved the accuracy while reducing the data to a more manageable size.

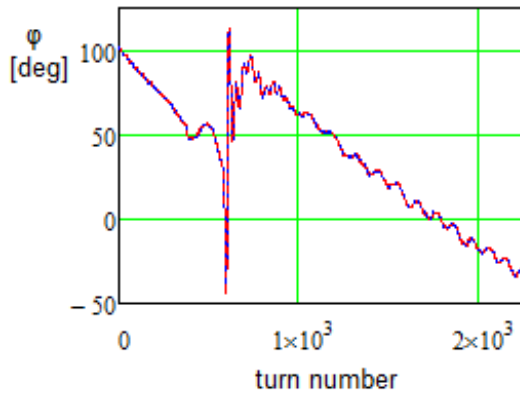


Figure 1: Phase difference between the bunch arrival time and rf zero crossing in vicinity of transition crossing; blue and red lines present two independent measurements with beam intensity of $4.82 \cdot 10^{12}$ particles.

The second phase of the analysis aimed at obtaining accurate calibrations for the rf voltage, rf phase and momentum offset. The measured phase difference between the bunch and rf voltage includes a shift due to a cable propagation delay. While the cable lengths for the RWM and RFSUM signals (10 mm/deg) are not known with sufficient accuracy to determine this delay directly, it may be determined by correction of the associated phase shift which is linearly dependent on the rf frequency: $\Delta\phi = 2\pi f_{RF} \Delta T$. Here ΔT is the difference in cable length expressed as a signal propagation delay. The linear dependence is clearly seen in Figure 1.

Using the RPOS signal, ΔT as well as an accurate calibration for RFSUM may be obtained by a procedure that will be now described. Knowing the accelerating phase (ϕ_{acc}), the rf voltage (V_n), and the beam deceleration due to resistive part of impedance (V_{bn}) one obtains the dependence of the beam energy (and consequently the momentum

deviation on turn $n+1$,

$$E_{n+1} = E_n + e \left(V_n \sin(\phi_{acc_n}) - V_{bn} \right), \quad V_{bn} = A_V N_p / \tau_{bn}, \quad (1)$$

Here τ_{bn} is the measured rms bunch length, N_p is the number of particles in the beam and A_V is a constant directly related to the effective longitudinal impedance. The assumed dependence of V_{bn} on τ_{bn} implies that the resistive part of the impedance has a weak dependence on frequency over a wide frequency range. This assertion is supported both by impedance measurements [1] and by analytical theory [2]. By combining the predictions of Eq. (1) to the measurements, one can extract ΔT , A_V , and the scaling factors for the RFSUM and RPOS signals. Note that since the revolution frequency changes mostly at low energy, the data collected at injection is much more sensitive to variations in ΔT .

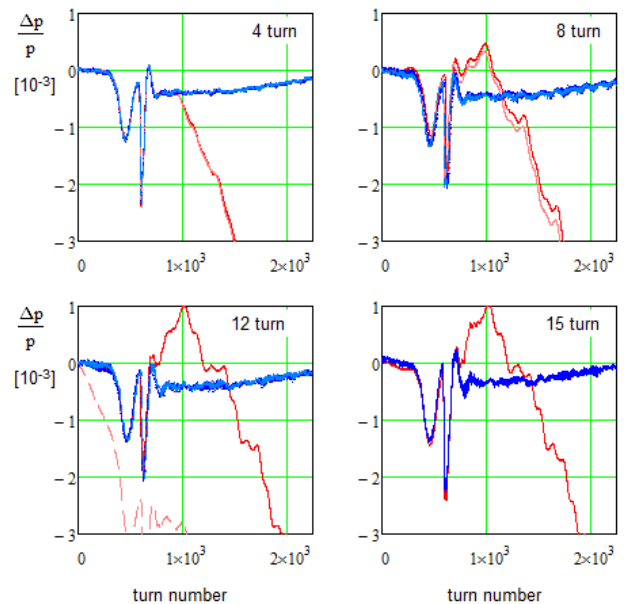


Figure 2: Predicted (red) and measured (blue) momentum offsets in vicinity of transition crossing for different beam intensity measured in number of injection turns; 4, 8, 12 and 15 turns correspond to $[1.17, 2.48, 3.78, 4.82] \cdot 10^{12}$ particles. For each intensity two measurements are shown.

Results of the fitting procedure for all measured data are presented in Figure 2. Good agreement between measurements and predictions is achieved below transition. Above transition, the poorer fit is caused by small systematic errors in the accelerating phase: the observed discrepancy corresponds to approximately 0.5 degree of error in accelerating phase. A probable source for this error is the difference between the accelerating phase determined as the center of rf bucket and the measured synchronous phase determined as a bunch centroid. The sign of this difference changes at transition due to changed symmetry of accelerating bucket. The difference is estimated to be on the order of 0.25 deg. Because the bucket left-right symmetry is inverted at transition, the error is effectively doubled. The error amounts to 2% of the ~ 12 deg rms bunch length near transition. The procedures outlined below provided calibrations for the rf voltage and rf phase well within 1% and

1 deg, respectively. This accuracy is sufficient for reliable simulations of transition crossing [2].

The left pane in Figure 3 shows the accelerating phase variation in the vicinity of transition for different intensities. The beam deceleration arising from the resistive part of the impedance causes a shift of the accelerating phase toward on-crest acceleration as the beam intensity increases. Averaged values of this shift, referenced to the rf voltage for a beam intensity of $1.17 \cdot 10^{12}$ are presented in the right pane of Figure 3. As expected, the phase shift exhibits a linear dependence on intensity; furthermore, the slope is consistent with the measured and predicted values of the real part of the wall impedance. It should be mentioned that Figure 3 incorporates rf voltage corrections to account for minor changes in accelerating voltage due to incomplete beam loading compensation by local cavity feedbacks. Without these corrections, the linear dependence of the phase shift on intensity is not nearly as clear.

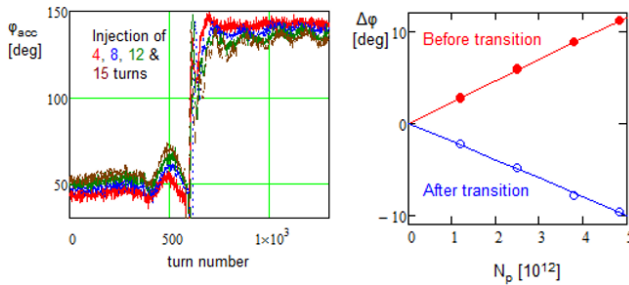


Figure 3: Accelerating phase variations in vicinity of transition crossing for different beam intensities (left) and corresponding shift of accelerating phase before and after transition crossing with beam intensity.

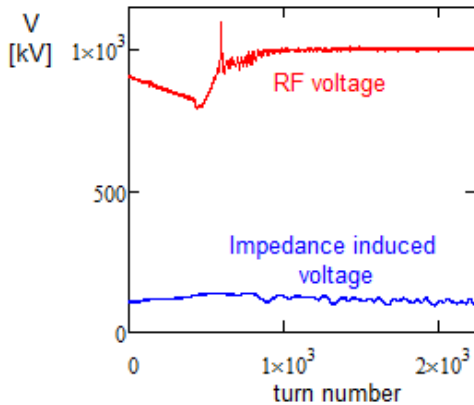


Figure 4: Dependence of rf voltage amplitude and impedance induced decelerating voltage averaged over bunch on the turn number in vicinity of transition crossing for beam intensity of $4.82 \cdot 10^{12}$ particles.

The large swing in accelerating phase well visible in Figure 1 is out of scale on Figure 3. This phase swing originates from the abrupt change in beam loading associated with the transition phase jump which is faster than the response time of the cavity feedback. As shown in Fig. 4, a corresponding spike in the rf voltage amplitude is clearly visible. The impedance induced voltage represents about 15% of the rf voltage amplitude.

SIMULATIONS

The rf voltage and accelerating phase extracted from measurements were used as input for the simulations described in Ref. [2]. However, two important parameters could not be directly measured.

The first one is the exact timing of the transition crossing. Simulations show that altering the transition crossing timing relative to the rf waveform by 10-20 turns has a significant effect on the rms bunch length above transition. Experimental data indicates that the transition jump timing jitter is on that order. From a simulation point of view, this prevents a precise determination of the exact moment at which transition occurs. It also suggests that reduction of the jitter would be beneficial.

The second parameter is the second order slip factor, η' , defined by the following equation:

$$\Delta T / T = \eta(\Delta p / p) + \eta'(\Delta p / p)^2 + \dots$$

Presently, no reliable procedure is available to accurately determine the second order slip factor at transition. Direct measurements would be very challenging. Potentially, the second order slip factor could be obtained using modern map based techniques but there is considerable uncertainty in the non-linearity of Booster magnets. Note that a change in η' on the order of ~ 0.05 significantly affects the rms bunch length variations above transition.

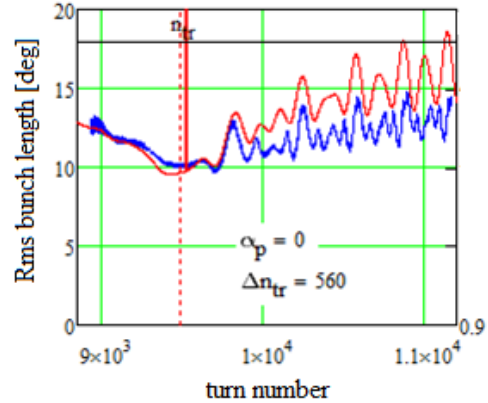


Figure 5: Dependence of rms bunch length on turn number in vicinity of transition crossing: blue – measurements, red – simulations; beam intensity of $4.82 \cdot 10^{12}$ particles.

With manual adjustment of the transition timing and second order compaction factor, simulations yield good agreement with the measurements. Figure 5 compares the measured to simulated rms beam sizes. The rms size extracted from the measurement data is systematically smaller after transition because the Gaussian fit algorithm used to extract the rms size excludes the long tails that develop in the longitudinal profile after transition. Figure 6 shows the computed profile and the decelerating voltage due to impedance before and after transition. The tail elongation after transition crossing is obvious. The decelerating voltage at transition reaches 30% of the accelerating voltage; this implies that any further intensity increase would require additional cavity voltage.

At PIP-II design intensity of $6.5 \cdot 10^{12}$, simulations at this stage suggest that with minor improvements it should be

possible to cross transition with a relative emittance increase comparable to the one observed under present operational conditions. That said, an issue that has been omitted from our simulations is the possibility of a microwave instability developing shortly after transition. While simple formulas provide estimates for intensity thresholds and growth rates, credible simulations require special attention to distinguish an actual instability from the intra-bunch motion excited by numerical noise.

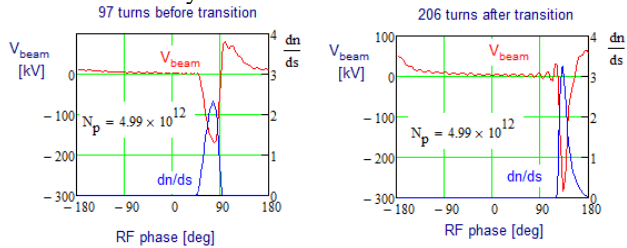


Figure 6: Longitudinal bunch density and beam induced voltage shortly before (left) and shortly after (right) transition crossing.

ACKNOWLEDGMENT

The authors wish to thank the Booster Department and the Operations Group for their support in acquiring machine data.

REFERENCES

- [1] J. Crisp, <http://beamdocs.fnal.gov/AD-public/DocDB/ShowDocument?docid=408>
- [2] J.-F. Ostiguy, *et.al.* "Modeling longitudinal dynamics in the Fermilab Booster Synchrotron", proc. IPAC 2016, pp. 874-876